3-D Electromagnetic Monte Carlo l'article-in-Cell Simulations of Critical ionization Velocity Experiments in Space

J. Wang, R. Biasca*, and P.C. Liewer
Jet l'repulsion Laboratory, California institute of Technology
*Nor theastern University, Boston, MA

Abstract

Although the existence of the critical ionization velocity (Cl V) is known from laboratory experiments, no agreement has been reached as to whether Cl V exists in the natural space environment. in this paper we move towards more realistic models of Cl V and present the first fully three-dimen sional, electromagnetic l'arLicle.-in-Ccll Monte-Carlo Collision (PIC-MCC) simulations of typical space-based CIV experiments. in our model, the released neutral gas is taken to be a spherical cloud traveling across a magnetized ambient plasma. Simulations are performed for neutral clouds with various sins and densities. The effects of the cloud parameters on ionization yield, wave energy growth, electron heating, momentum coupling, and the 3-D structure of the newly ionized plasma are discussed. The simulations suggest that the quantitative characteristics of momentum transfers among the ion beam, neutral cloud, and plasma waves is the key indicator of whether CIV can occur in space. The missing factors in space-based CIV experiments may be the conditions necessary for a continuous enhancement of the beam ion momentum. For a typical shaped charge release experiment, favorable CIV conditions may exist only in a very narrow, intermediate spatial region some distance from the release point due to the effects of the cloud density and size. When CIV does occur, the newly ionized plasma from the cloud forms a very complex structure clue to the combined forces from the geomagnetic field, the motion induced emf, and the polarization. Hence, the detection of Cl V also critically depends on the sensor location.

1 Introduction

Critical ionization velocity (CIV) was first proposal by Alfvén in his theory of the formation of the solar system [*Alfvén*,1 954]. Alfvén hypothesized that a neutral gas propagating across a magnetized plasma will undergo an anomalous ionization when the relative velocity between the neutrals and the plasma exceeds a certain critical velocity given by

$$v_c \, , \quad \sqrt{\frac{2e\phi_{ion}}{m_n}} \tag{1}$$

where ϕ_{ion} and m_n are the ionization) potential and mass of the neutral atom, respectively. Over the past forty years, the critical ionization velocity phenomenon has been the subject of many space experiments (see, for example, *Haerendel, 1982; Torbert and Newell, 1986; Wescott et al.*, 1986; *Stenback-Nielsen et al.*, 1990a; Stcnback-Nielsen *et* d., 1990b; *Torbert et. al.*, 1992), laboratory experiments(*A xnäs, 1978; Brenning*, 1981; *Danielsson, 1970; Danielsson and Brenning*, 1975; *Axnäs and Brenning*, 1990), and theoretical and numerical studies (*Machida and Goertz*, 1988; *Machida et al*, 1988; *Biasca et al, 1992, 1993; Moghaddam-Taaheri*, 1994; *Okuda and Chouciri, 1994)*. Previous studies have led to the following generally accepted CIV sequence: (1) seed ionization of the neutral cloud forms a weak ion beam drifting across a magnetic field, (2) the ion beam induces a modified beam-plasma instability, (3) the instability transfers energy from the ion beam into electron energy, (4) the electrons are heated to energies above the neutral's ionization energy, (5) further neutrals arc ionized by electron impact ionization, reinforcing the ion beam and leading to a positive feedback loop. Although the existence of CIV has been verified in a series of laboratory experiments, the. results of space-based CIV experiments have in general been inconclusive or negative. No general agreement has been reached as to whether CIV exists in th c natural space environment.

The cost and complexity of space experiments precludes the possibility of performing the parametric studies needed to determine the missing factor in achieving CIV in space. Wall effects and the difficulty of matching space conditions in a laboratory experiment make it difficult to extrapolate laboratory simulations to the space environment. Overall, numerical simulations based on first principles perhaps provide the best means of understanding CIV process at reasonable cost.

In previous studies, one- and two-dimension al particle-in-eel] simulations with Monte-Carlo charged particle-neutral collisions (PIC-MCC) have been developed to study CIV. For instance, *Machida and Goertz [1 988], Machida et al [1* 988], and *Biasca et al* [1 992; 1993] studied the CIV

process for a periodic system of an infinite neutral gas beam propagating in a homogeneous plasma. The finite size of the cloud most likely plays an important role in CIV. Recently, *Moghaddam-Taaheri et al [1* 994] and *Okuda and Choueiri* [1994] conducted 2-D simulations to study CIV for a finite size neutral cloud. in *Moghaddam-Taaheri et al* [1994], three-dimensional (3-I)) effects were studied using 2-D simulations performed in 2 separate planes. With the exception of *Machida and Goertz* [1*988],* all previous simulations have been electrostatic.

Although these studies have added greatly to the understanding of the CIV, their results cannot be easily extended to space-bascc] Cl V experiments. This is because the CIV experiment is fund amentall y a 3-dimensional phenomen a. Many of the space experiments which do indicate enhanced ionization levels (supposedly due to Cl V interactions), result in ions appearing further from the release point than should be expected from previous theoretical and numerical work (*Biasca et al., 1* 993). The overall ionization level observed also tends to be much less than might be expected from purely theoretical reasoning. Onc possibility for these discrepancies between experiments and theory is that, in a 3-D situation, the ion beam may not get reinforced as easily as that in a 1-D or 2-D situation clue to greater effects of the finite cloud size on the efficiencies of momentum and energy transfers among the ion beam, the neutral cloud, and the background plasma. This can restrict the CIV process. Another possibility is that the newly forming plasma polarizes and causes downstream, cross-field transport of the new plasma. This cross-field transport of the plasma may well have important implications for both the level of ionization obtained in CIV experiments and the observed position where the ionization occurs. Overall, the importance of polarization and momentum coupling is not yet well understood. It is clear, however, that the calculation of momentum transfers among a finite size cloud, an ion beam, and a magnetized plasma, and the study of the dynamics and polarization of the newly forming plasma are beyond the reach of a 1- or 2-D simulation model. They can only be achieved using fully 3-dimensional particle simulations.

in this paper, wc move towards more realistic models of Cl V and present the first fully three-dimensional, electromagnetic PIC-M CC simulations of typical space-ba.ml CIV experiments. Results arc presented for neutral clouds with different sizes and densities. The simulation results suggest that whether CIV can occur in space depends on the quantitative characteristics of momentum and energy transfers among the ion beam, neutral cloud, and plasma waves. The missing factors in space-based CIV experiments may be the con ditions necessary for a continuous enhancement of the beam ion momentum. When Cl V dots occur, the newly ionized plasma from the

cloud form a complex structure due to the combined forces from the geomagnetic field, the motion induced emf, and the polarization. We find that the ion beam momentum provides a better indicator of CIV than the electron temperature.

Our simulation model is described in Section 2. in section 3, wc study CI V interactions for a finite size cloud and discuss effects of neutral cloud density and size on the CIV process as well as the dynamics of ionized plasma cloud. Section 4 contains practical implications and a conclusion.

2 Simulation Model

Figure 1 shows our simulation model for a typical neutral gas release experiment in the ionosphere. in the model, the released neutral gas is taken to be a spherical cloud traveling with a constant velocity $\vec{v}_n$ in the x direction across a collisionless, magnetized background plasma. When a plasma particle impinges upon the neutral cloud, a collision may occur. The geomagnetic field $\vec{B}_0$ is mainly in the z direction.

Wc have developed a fully 3-D electromagnetic 1'1 C-MCC code which follows both ambient and newly ionized electrons and ions to simulate this system. In the code, plasma particles arc pushed using a standard relativistic particle push; currents arc deposited using a rigorous charge conservation scheme[*Villasenor and Buneman*,1 *992];* and the self-consistent electromagnetic field is solved using a local finite-cliffcrcncc time-domain solution to the full Maxwell's equations. Interested readers arc referred to *Wang et al*[1 994] for detailed discussions of the electromagnetic PIC part of the code. For those plasma particles that impinge upon the neutral cloud, a Monte-Carlo collision subroutine similar to that in *Machida and Goertz*[1 *988]* aud *Biasca et al*[1 992] is called to determine whether a collision has occurred and to calculate the particle's velocity after the collision.

The simulations may be conducted either in the rest reference frame of the ambient plasma or in the reference frame fixed with the neutral C1OUC1. Initially, the background plasma is a quiet Maxwellian distribution (Te_0 and Ti_0 for the ambient electron and ion temperature, respectively). At the start of the simulation, the neutral C1OUC1 is set to drift across the plasma with some seed ions within it. In reality, the seed ions arc produced either by photoionization or charge-cxchaugc collisions. (If the cloud reference frame is used, then the ambient plasma is injected into the system with a drifting velocity - $\vec{v}_n$, aud an electric field due to the change of the reference frame, $\vec{v}_n$ x $\vec{B}_0$, is applied to the background,) For the boundary conditions, those background plasma

particles that flow out of the simulation domain are refreshed with the ambient temperature, T_{e0} or T_{i0}, before they are injected back to the simulation domain. If any newly ionized plasma particles reach the boundary of the simulation domain, they are deleted from the particle list. Currently, a periodic boundary condition is used for the electromagnetic field. Since the largest wave amplitude in the system remains concentrated near the cloud [*Okuda and Choueiri*, 1 *994],* the use of the periodic boundary condition on the fields should only have a negligible effect on the results if the simulation domain is large enough. Since the waves excited in. this problem have a much larger wave length along B_0, we are unable to set a simulation domain large enough in the B_0 due to computational restrictions. Hence, the periodic boundary condition in the z direction may have some effects in terms of affecting the instability growth rate. However, this would not change the overall mechanism.

To make the problem more tractable, in the simulations presented here, we only include the electron-neutral ionization collision, the most important collisional process for CIV. Similar to *Machida and Goertz*[1 *988], we* model the electron-neutral collision frequency ν_{e-n} as a step function with a low-energy cut-off:

$$\nu_{e-n} = \nu_{ion} \; if \; \frac{1}{2} m_e (\vec{v}_e - \vec{v}_n)^2 \geq e\phi_{ion}; \quad \nu_{e-n} = 0 \; otherwise$$

where $\nu_{ion} = n_n < \sigma_{ion} v_e >$ is taken as au input parameter. In addition, we also take the neutral cloud density n_n, radius r_n, and drifting speed v_n as constant. These are reasonable assumptions for the relatively small spatial and time scale of the simulation. The effects of the neutral cloud size and density are studied via a parametric study on r_n and ν_{ion} (ν_{ion} is directly proportional to the neutral density.).

in this paper, we present results from 4 simulation cases (Table I). The ionization collision frequency is taken to be $\hat{\nu}_{ion} = \nu_{ion}/\omega_{pe} = 0.2$ in cases 1a and lb, and $\hat{\nu}_{ion} = 0.05$ in cases 2a and 2b. Cases la and 1b represent a dense neutral cloud, and cams 2a and 2b represent a more rarefied neutral cloud. in cases 1 a and 2a, we consider a smaller cloud with a radius $\hat{r}_n = r_n/\lambda_D = 15$. In cases 1 b and 2b, we consider a larger cloud with $\hat{r}_n = 25$.

1 Depending on the problem size aud the reference frame used in the simulation, the number of grid points used for the simulation domain is in the range of $L_x = 40 - 100$, $L_y = 40 - 60$, and $L_z = 40 - 60$, and the number of ambient plasma particles initially loaded is in the range of $N_0 \sim 1\,0^6 - 1\,0^7$ (about 34 parLicles/cell). Some seed ions are also randomly distributed within the cloud at the start of the simulation, The number of seed ions is $N_{seed} \simeq 450$ for $\hat{r}_n = 15$ and $N_{seed} \simeq 2090$ for $\hat{r}_n = 25$ (about 4 seed ions/cell within the cloud). The neutral drifting

velocity is taken to be $v_n/v_c = 4$ and the initial electron thermal velocity is chosen such that $\frac{1}{2}m_e v_{e0}^2 \simeq 0.098 e\phi_{ion}$. Due to computational restrictions, an artificial ion mass of $m_i/m_e = 100$ is used for the seed, ambient, and newly born ions. Other simulation parameters are listed in Table '2. They arc comparable to those used in previous CIV simulations (e.g. *Machida and Goertz* 1988, *Machida et al* 1988, etc.).

3 Results and Discussions

We first examine the spatial distribution of the plasma ionized from the neutral cloud. In Figure *2 wc show* two snapshots each for simulation cases 1 a and 2a ($\hat{r}_n = 25$). The left column shows case la ($\hat{\nu}_{ion} = 0.2$) and right column shows case 2a ($\hat{\nu}_{ion} = 0.05$). In both columns, the top panels are taken when the simulation is in a very early stage ($t\omega_{pe} = 6$). The lower panels are taken at $t\omega_{pe} = 200$. in the figure, the white particles represent neutrals, blue particles represent newly born electrons ionized from the cloud, and yellow particles represent newly born ions. The ambient plasma, which maintains the charge neutrality, is not shown. The left column shows that the plasma ionized from the neutral cloud evolves to form an "asymmetric sphere-tail" structure. The newly born ions mainly drift with the neutral cloud because they are only weakly magnetized. Driven by the motional induced emf, the newly born ions also expand in the $\vec{v}_n \times \vec{B}_0$ direction as they drift along with the neutral cloud. Since the electrons are strongly magnetized, the newly born electrons arc trapped by the magnetic field and form a curved tail trailing the neutral cloud. Since the electrons can move freely along the magnetic field line, this tail spreads along $\vec{B}_0$ like a sheet. The right column (case 2a) also shows a similar structure for the newly born plasma. However, th c "asymmetric sphere-tail") structure is less obvious because there is much less plasma created from the neutral cloud in case 2.

We next study in detail the important quantities associated with CIV. Figure 3 shows the time history of the ionization yield for the four simulation cases. (Since cases 1a and 2a have a larger problem size, wc arc unable to run cases la and 2a as long as cases 1b and 2b.) Here, the ionization yield is defined as Ne_{new}/Ne_0, where Ne_{new} is the total number of the newly born electrons and Ne_0 is the number of ambient electrons initially contained within the neutral cloud, $Nc(I = n_{e0}V_{cloud} = n_{e0}\frac{4}{3}\pi r_n^3$ In our simulations, the number of ambient electrons initially within the cloud is $Ne_0 \simeq 1923$ for $\hat{r}_n = 15$ and $Nc_o \simeq 9027$ for $\hat{r}_n = 25$.

The ionization yields for case 1a and 1 b, shown on the top panel of figure 3, clearly exhibit an

exponential growth. The exponential growth starts at about $t\omega_{pe} \sim 100-150$. At $t\omega_{pe} = 100$, the ionization yield is only $Ne_{new}/Ne_0 \simeq 0.87$ for case 1a aud $Ne_{new}/Ne_0 \simeq 0.72$ for case lb. By the end of the case 1 simulation, at $t\omega_{pe} = 232.5$, we find $Ne_{new}/Ne_0 \simeq 6.2$ for case la. By the end of the case 2 simulation, at $t\omega_{pe} = 400$, we find $Ne_{new}/Ne_0 \simeq 28$. for case 1b. This exponential growth indicates that an anomalous ionization process is in process. The ionization yields for case 2a and 2b, shown on the bottom panel, also show some signs of exponential growth. However, the growth rate is at a much weaker level (note there is a factor of 10 scale difference between the top and bottom panels).

Figure 4 shows the time evolution of the wave energy associated with the electric and magnetic fields within the cloud. In the calculation, the electric and magnetic field is normalized as

$$\hat{E} = \frac{eE}{m_e d_{cell} \omega_{pe}^2}, \quad \hat{B} = \frac{eB}{m_e d_{cell} \omega_{pe}^2}$$

The wave energy is calculated as

$$\frac{\delta \hat{E}^2}{2} = \frac{1}{V_{cloud}} \Sigma \frac{(\hat{E} - \hat{E}_0) \cdot (\hat{E} - \hat{E}_0)}{2}; \quad \frac{\delta \hat{B}^2}{2} = \frac{1}{V_{cloud}} \Sigma \frac{(\hat{B} - \hat{B}_0) \cdot (\hat{B} - \hat{B}_0)}{2} \tag{2}$$

where the summation is for all the grid points within the cloud region.

The top panel shows the wave energy for cases 1 a and 1 b while the bottom panel shows cases 2a and 2b. An exponential growth of $\delta \hat{E}^2$ is present in all cases, while $\delta \hat{B}^2$ remains near zero. The rapid growth of the electric field wave energy indicates that au instability of electrostatic nature has been excited. This is exactly the modified beam-plasma instability induced by the ion beam within the cloud. When ν_{ion} is the same, the instability grows faster for the larger cloud. 'This is apparently because the smaller cloud size imposes a more severe restriction on the wave length of the unstable wave modes allowed, which limits the instability growth rate. According to linear stability theory, the maximum growth rate should occur for wavelengths along the magnetic field of $\lambda_{m,||} = \sqrt[4]{\frac{m_i}{m_e}} \frac{v_n}{f_{LH}}$ where m_i and m_e are the mass Of the electron and ion, respectively, and f_{LH} is the lower hybrid frequency [*Moghaddam-Taaheri et al,, 1* 994]. If the cloud is not large enough to contain the most unstable mode, it seems plausible that the growth rate of the instability will be reduced [*Newell*, 1985]. Although this has never been shown rigorously due to the theoretical problems of handling the necessary non-uniform plasma, recent numerical work has indicated the reduction in the growth rate dots indeed occur [*Moghaddam-Taaheri et al., 1994]*. Because of the computational restrictions needed to carry out the full three dimensional simulations, all the simulations here usc clouds with $r < \lambda_{m,||}$, i.e. the size of the cloud is smaller thau the wavelength alon g the magnetic field needed for maximuro growth of the instability. Hence, our simulations

represent early stages of space based CIV experiments when the cloud is still small. The reduced ionization rate in the smaller cloud agrees with the trend of smaller cloud sizes reducing the instability growth rate and hence the ionization rate obtained through the CI V proces.

A very distinct difference is noticable when comparing cases 1a and 1b to cases 2a and 2b. The instability is much stronger in cases 1 a and 11> than in cases 2a and 2b. The combined results of the ionization yield and wave energy clearly suggest that critical velocity ionization has occurred in cases 1 a and 1 b. For cases 2a and 2b, the much weaker growth of the ionization yield and the wave energy only indicates signs of marginal CI V.

Electron heating by unstable waves is regarded as a key step to ignite CI V. in all CI V experiments, the electron temperature enhancement has been used as a key indicator for Cl V. We next examine electron heating in our simulations. Figure 5 shows the time history of the electron temperature within the neutral cloud region. The temperature Te is calculated using all electrons inside the cloud region and is normalized by Te_0, the initial electron temperature. We find rapid increase of T_e starts at $t\omega_{pe} \sim$ 100, which is consistent with the instability growth and ionization yield growth shown in figures 3 and 4. However, it is interesting to observe that, while strong electron heating continues through the simulation course in cases 2a and 2b (which only have marginal signs of CIV), electron heating reaches a semi-steady state at a modest level of $Te/Te_0 \sim 2$ at $t\omega_{pe} \sim 180 - 200$ in cases 1 a and 1 b (which have clear signs of CIV). This is apparently due to the trade off between electron heating rate and the collision frequency. in a collisionless plasma, electron temperature enhancement is directly correlated with the instability level. However, when e]ectron-neutral collisions are present, the collision frequency imposes an "windowing effect" upon electron heating. In a plasma with a lower collision frequency, an electron will heat longer and reach a higher temperature before colliding with a neutral, ionizing and losing its energy. On the other hand, if the collision frequency is high, the electrons collide and excite neutrals so often that Te can only reach a very moderate level no matter how strong the instability is. Hence, although the electron temperature is an important parameter to measure in a CIV experiment, we find that strong electron heating does not necessarily indicate CIV. We note, in most space-based CIV experiments, strong electron heating but no significant, ionization yield are present at the same time.

One of the most important mechanisms in a CIV process is the momentum coupling among the neutral cloud, the ion beam, and the ambient plasma [*Haerendel*, 1982]. The momentum coupling determines whether the initial ion beam momentum can get reinforced so the process is

in a positive feedback loop leading to CIV. In Figure G, we plot the time history of the beam ion momentum in the drifting direction for all simulation cases. The initial ion ham momentum is that of the seed ions

$$P_{x0} = N_{seed} m_i v_n \tag{3}$$

The beam ion momentum at a later time is that of the initial seed ions and all newly born ions.

$$P_x = \Sigma_{N_{seed}+N_{new}} (m_i v_i) \tag{4}$$

If we consider a finite size cloud of ions drifting in a plasma with no collisional interactions between the ion cloud and the plasma, the ion cloud will initially excite some electromagnetic waves in the plasma at the expense of losing its momentum. Since there is no mechanism to supply the ion beam momentum, th c wave-particle interactions will eventually consume all the initial ion momentum, and the ion cloud will stop and the waves will disappear. For a very rarefied n eutral cloud where electron-n eutral collisions have a negligible effect, the process is similar. in Figure 6 we also plot the beam ion momentum for a very rarefied neutral cloud, where the collision frequency is $\hat{\nu}_{ion} = 0.001$ and the radius is $\hat{r} = 15$. As the result shows, the beam ion momentum P_x for this cloud quickly decreases to zero,

The collisional interaction between electrons and the neutral cloud provides the mechanism to resupply the ion beam momentum lost via wave excitation. When $P_x/P_{x0} > 1$, the process is in a positive feedback loop. Clearly, in order for sustained CIV to occur, the collisions and wave particle interaction must result in a process such that

$$P_x/P_{x0} > 1, \quad and \quad d(P_x/P_{x0})/dt > 0 \tag{5}$$

As shown in Figure 6, these two conditions are well satisfied for cases la and lb. For case 2a, eq(5) is marginally satisfied, and for case 2b, eq(5) is not always satisfied. These results are consistent with the results shown in Figures 3 and 4, where we found case 1 has clear signs of Cl V and case 2 only has marginal signs of CIV.

We find the quantitative characteristics of the beam ion momentum, rather than electron heating, is the most important indicator for Cl V. The conditions that can result in a process with $P_x/P_{x0} > 1$ and $d(P_x/P_{x0})/dt > 0$ are the sufficient conditions for CIV. Unfortunately, these conditions are not known a *prior*, which may be the missing factors in space-based CIV experiments.

4 Conclusions

We have developed a 3-D Cl V interaction model based on electromagnetic PIC-MCC simulations. The model has been used to simulate space based Cl V experiments. In this paper, we have focused our discussions on the effects of the cloud size and the electron-neutral collision rate on ionization, wave energy growth, electron heating, momentum coupling, aud the 3-D structure of the newly ionized plasma.

Our simulations have some interesting practical implications for space based CIV experiments. We find while space based CIV experiments are designed to satisfy the necessary conditions of CIV, they do not necessarily result in au interaction process with the continuous enhancement of the ion ham. The quantitative conditions that will result in a process satisfy in g eq(5), which may be the sufficient conditions for CIV to occur in space, are still not clear. Nevertheless, our simulations suggest that, in gen eral, the replenishment of the beam ion momentum is more easily achieved for larger cloud size and higher neutral density. This suggests that, for a typical nozzle release experiment, favorable Cl V condition may exist only in a very narrow, intermediate region some distance from the release point. Figure 7 qualitatively illustrates the neutral cloud size and neutral density profile as a function of the distance between the cloud and the nozzle exit. Near the nozzle exit, where the neutral density is sufficiently large, the cloud size is often too small to support the unstable waves, which limits the growth of the instability and thus, the energy transfer from the beam ions to the electrons. Far away from the nozzle exit, where the cloud has expanded to a sufficiently large size, the neutral density is too low to allow the collision frequency that is needed for sustained beam momentum enhancement and thus, ionization. When CIV does occur, wc find the newly ionized plasma from the cloud forms a very complex structure, appearntly duc to the combined forces from the geomagnetic field, the motion induced emf, and the polarization. Significant plasma density enhancement is likely to be detected only in the core region of the neutral c1ouc1. Hence the detection of Cl V critically depends on the sensor location.

The simulations presented here used a relatively simple neutral cloud model. The major limitation of the current model is imposed by th c computer memory and cost, which restricted our simulations in relatively small scale and artificial ion mass ratio. Currently we are in the process of incorporating a more sophisticated neutral cloud model and implementing our model onto massively parallel supercomputers (i.e. Intel Paragon and Cray T3D) for larger scale, more realistic simulations.

Acknowledgment: We would like to acknowledge many useful discussions with Gerald Murphy, David Cooke, and Nils Brenning. We also thank Eric Mattson for helping to produce the color figure (Fig 2). This research was carried out at the Jet, Propulsion Laboratory under a contract with NASA. One of the authors (RB) acknowledges the support of the Air Force Geophysics Fellowship. The Cray Supercomputer used in this study was provided by the JPL Supercomputing project and NASA.

References

[1] Alfven, H., *On the Origin of the* Solar *System*, Oxford University Press, New York, 1954.

[2] Axnäs I. Experimental investigation of the Critical Ionization Velocity in Gas Mixtures. *Astrophys. Space Sci.*, *55*, 139, 1978.

[3] Axnäs I. and N. Brenning, Experiments on the magnetic field and neutral density limits on CIV interaction. *Adv. Space res.*, *10*, *27, 1990.*

[4] Biasca, R., D. Hastings, aud D. Cooke, Simulation of the critical ionization velocity: effects of using physically correct mass ratio, *J. Geophys. Res.*, 97(5), 6451, 1992

[5] Biasca, R., D. Hastings, and D. Cooke, Upper bound estimates of anomalous ion production in space-based critical ionization velocity experiments, *J. Geophys. Res.*, 98(1 O), 17569, 1993

[6] Brenning N. Experiments on the Critical Ionization Velocity Interaction in Weak Magnetic Fields. *Plasma Phys.*, *23*, *967, 1981.*

[7] Danielsson H,. Experiment on the Interaction between a Plasma and a Neutral Gas. *Phys. Fluids*, *13*, 2288, 1970.

[8] Danielsson H,. and N. Brenning. Experiment on the interaction between a Plasma and a Neutral Gas. II. *Phys. Fluids*, *18*, *661,* 1975.

[9] Haerendel G. Alfvén's Critical Velocity Effect Tested in Space. *Z. Naturforsch*, 97, 728, 1982.

[10] Machida, S. and C. K. Goertz, The electromagnetic effect on the critical ionization velocity phenomena, *J. Geophys. Res.*, 93, 11495, 1988

[11] Machida, S., C.K. Goertz, and G. Lu, Simulation of the ionizing front in the critical ionization velocity phenomena, *J. Geomag. Geoelectr.*, 40, 1205, 1988

[12] Newell 1'. 'J'. Review of the Critical ionization Velocity Effect in Space. *Rev. Geophys.*, 29, 93, 1985.

[13] Stenbaek-Nielsen 11., E. Wescott, G. Haerendel, and A. Valenzuela. Optical Observations on the CRIT-II Critical Ionization Velocity Experiment. *Geophys. Res. Lett.*, *17*, 1601, 1990.

[14] Stcnbaek-Nielsen 11., E. Wescott, D. Rees, A. Valenzuela, and N. Brenning. Non-solar UV Produced ions Observed Optically from the Cl{,lJ'1 Critical Velocity ionization Experiment. *J. Geophys.Res.*, 95, 7749, 1 990.

[15] Torbert R., C. Kletzing, K. Liou, and D. Rau, Prompt ionization in the CRIT II barium release. *Geophys. Res. Lett.*, 19, 973, 1992,

[16] Torbert R. and I'. Newell. A Magnetospheric Critical Velocity Experiment: Particle Results. *J. Geophys. Res.*, *91*, 9947, 1986.

[17] Moghaddam-Taaheri, 1';., G.Lu,C.Goertz,and K.-I. Nishikawa,]'article-in-cell simulations of the critical ionization velocity effect in finite size clouds, *J. Geophys. Res.*, 99(4), 6393, 1994.

[18] Okuda, H. and E. Choueiri, Numerical simulation of neutral gas release experiments in the ionosphere, *Phys. Plasmas, 1 (5), 1669,* 1994,

[19] Villasenor, J., and O. Buneman, Rigorous charge conservation for local electromagnetic field solvers, *Computer Physics Comm.*, 69, 306, 1992.

[20] Wang, J., P. Liewer, and V. Decyk, 3-D electromagnetic plasma particle simulations on a MIMD parallel computer, to be published in *Computer Physics Communications*, 1994.

[21] Wescott E., H. Stenbaek-Nielson, and T. Hallinan. Star of Condor: A Strontium Critical Velocity Experiment, Peru, 1983. *J. Geophys. I/es.*, *91*, 9933, 1986.

simulations	$\hat{\nu}_{ion}$	$\hat{r}_n$
1a	0.2	25
1b	0.2	15
2a	0.05	25
2b	0.05	15

'l'able 1: Simulation cases

d_{cell}/λ_D	5
$dt\omega_{pe}$	0.125
m_i/m_e	100
ω_{pe0}/Ω_e	1
B_z/B_x	$\sqrt{m_i/m_e}$
v_n/Vc	4
v_n/v_{i0}	12.5
T_{i0}/T_{e0}	1

Table 2: Simulation parameters

Figure Captions

Figure 1: Schematic illustration of the simulation model. A neutral cloud with some seed ions travels across a magnetized background plasma.

Figure 2: Snapshots of the plasma ionized from the cloud from simulation cases la (left column) and 2a (right column). Top panels are taken at $t\omega_{pe} = 6$ and bottom panels are taken at $t\omega_{pe} = 200$. White particles: neutrals. Yellow particles: newly born ions. Blue particles: newly born electrons. The ambient plasma is not shown here.

Figure 3: ionization yield Ne_{new}/Ne_0. $Ne_0 \simeq 1923$ for $\hat{r}_n = 15$ and $Ne_0 \simeq 9027$ for $\hat{r}_n = 25$. Top panel: cases 1 a and 1b. Bottom panel: cases 2a and 2b. (Note the change in scale between case 1 and case 2)

Figure 4: Wave energy within the cloud. Top panel: cases la and 1b. Bottom panel: cases 2a and 2b. (Note the change in scale between case 1 and case 2)

Figure 5: Electron temperature Te/Te_0 within the cloud. Top panel: cases 1a and lb. Bottom panel: cases 2a and 2b.

Figure 6: Beam ion momentum P_x/P_{x0}.

Figure 7: Schematic illustrations of the neutral cloud size and density profile as a function of the distance between the cloud and the nozzle exit in typical nozzle release experiments.

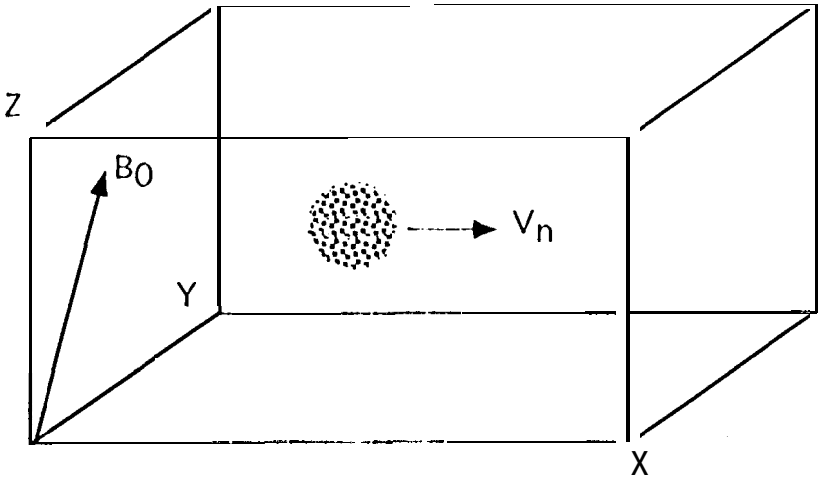

Figure 1

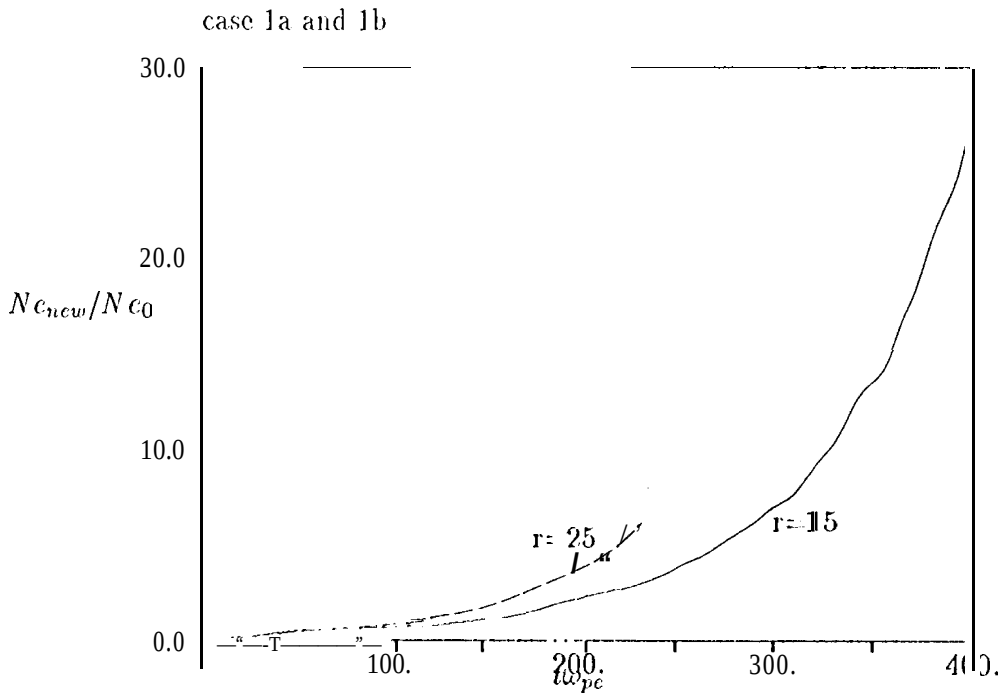
case 1a and 1b
30.0
20.0
Nc_{new}/Nc_0
10.0
0.0
r= 25
r=15
100.
200.
300.
$t\omega_{pe}$

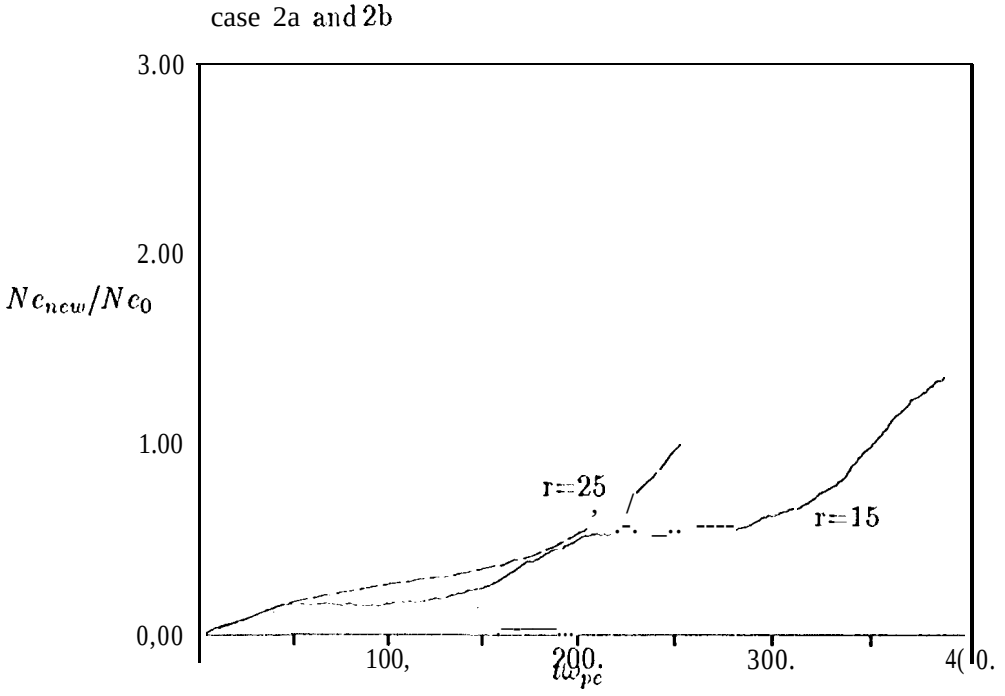
case 2a and 2b
3.00
2.00
Nc_{new}/Nc_0
1.00
0,00
r=25
r=15
100,
200.
300.
$t\omega_{pe}$

Figure 3

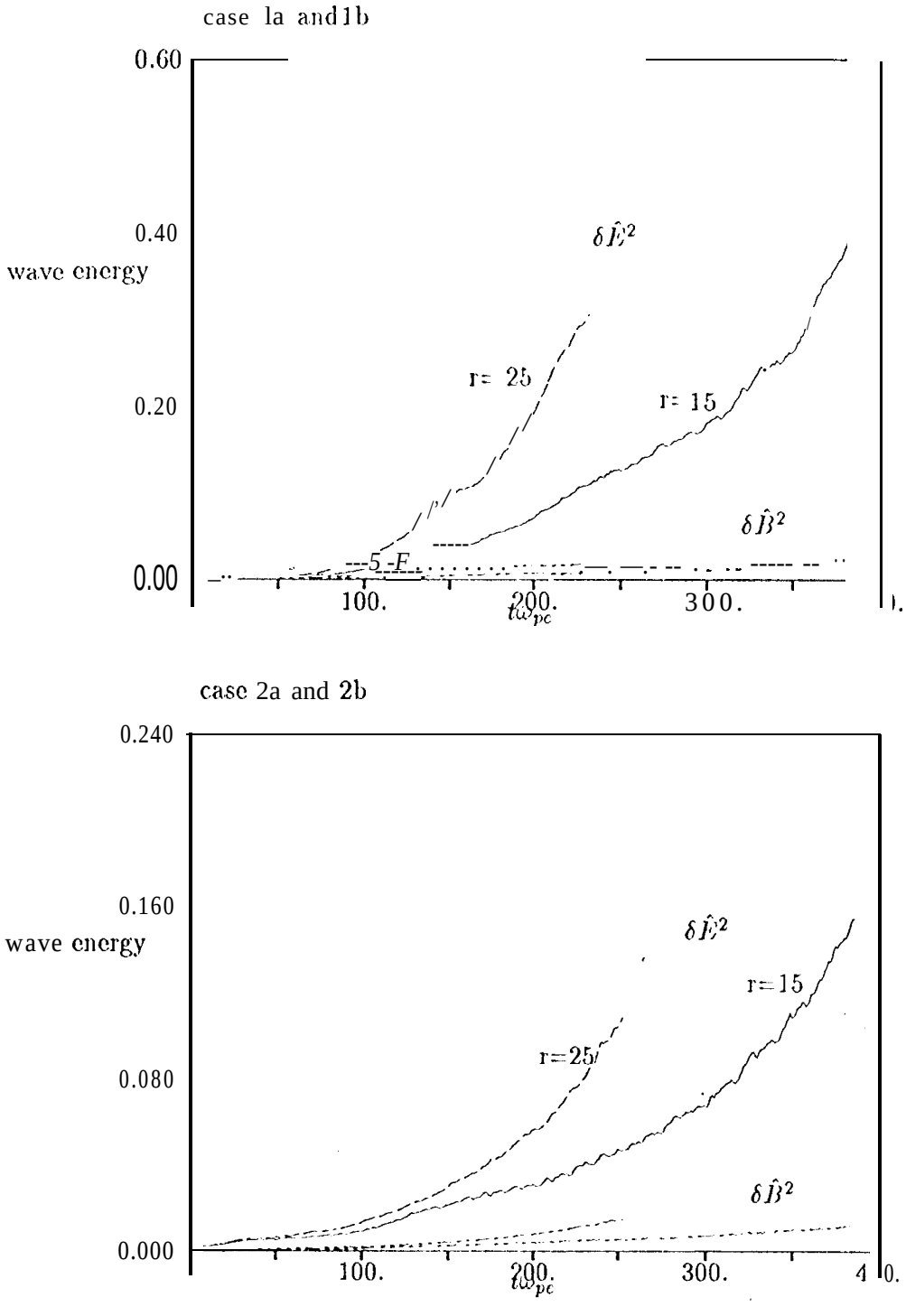
case la and1b
0.60
0.40
wave energy
0.20
0.00
$\delta\hat{E}^2$
r= 25
r= 15
$\delta\hat{B}^2$
5-F
100.
200.
300.
$t\omega_{pe}$
case 2a and 2b
0.240
0.160
wave energy
0.080
0.000
$\delta\hat{E}^2$
r=15
r=25
$\delta\hat{B}^2$
100.
200.
300.
$t\omega_{pe}$

Figure 4

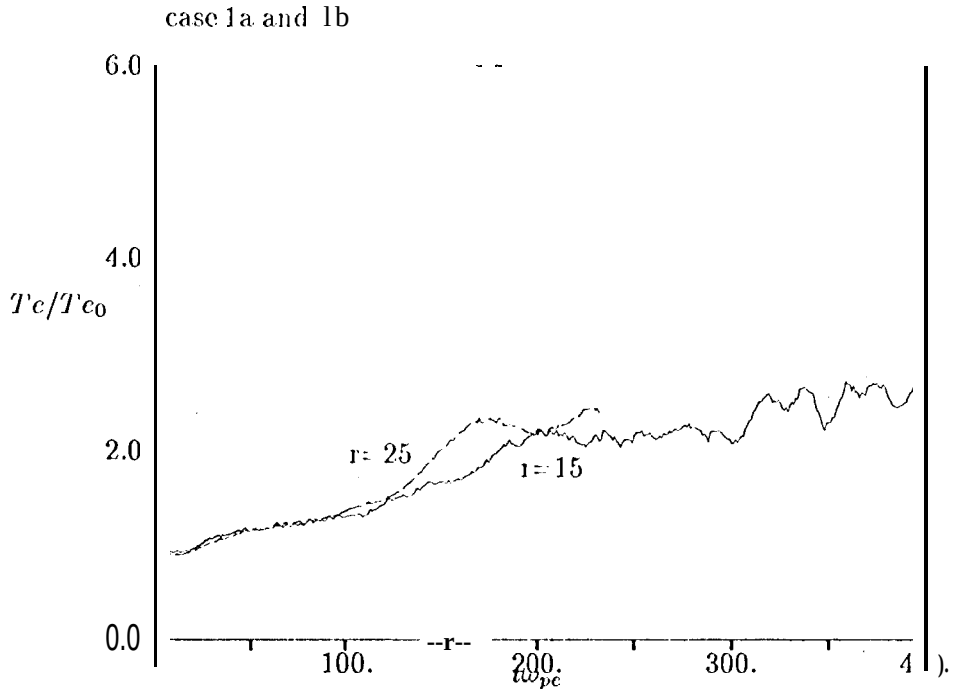
case 1a and 1b
6.0
4.0
2.0
0.0
Te/Te_0
r= 25
r= 15
100.
200.
300.
$t\omega_{pe}$

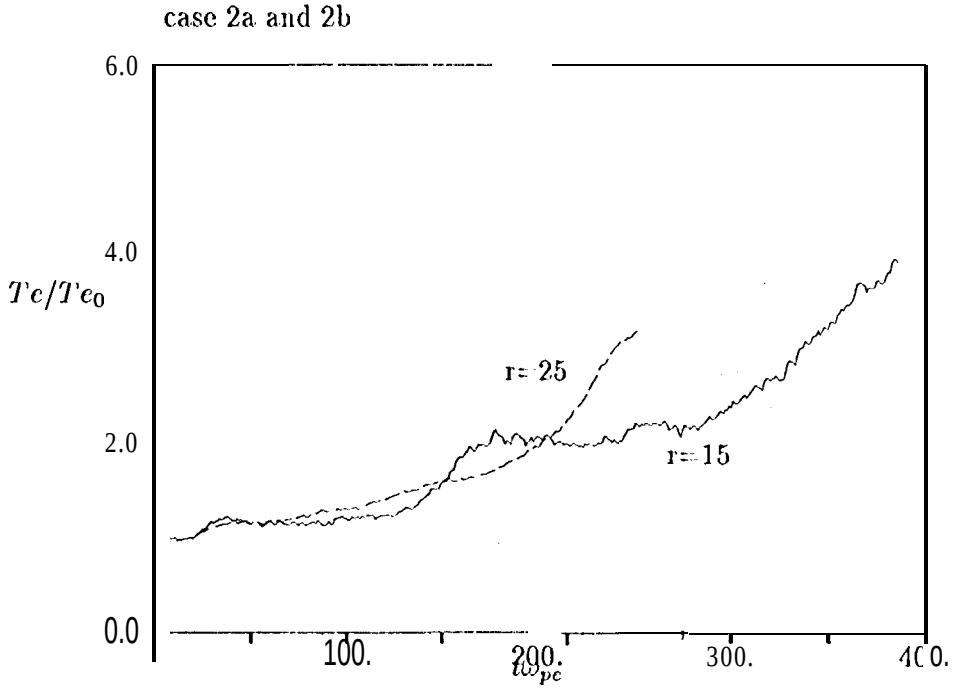
case 2a and 2b
6.0
4.0
2.0
0.0
Te/Te_0
r= 25
r= 15
100.
200.
300.
$t\omega_{pe}$

Figure 5

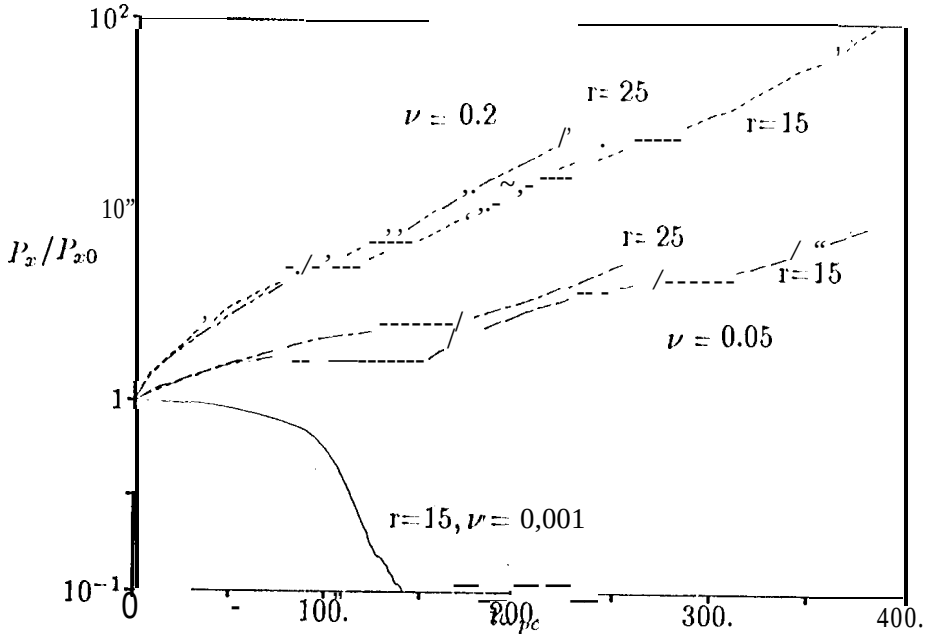
10^2
10^1
1
10^{-1}
P_x/P_{x0}
0
100.
200.
300.
400.
t/t_c
r= 25
ν = 0.2
r=15
r= 25
r=15
ν = 0.05
r=15, ν = 0,001

Figure 6

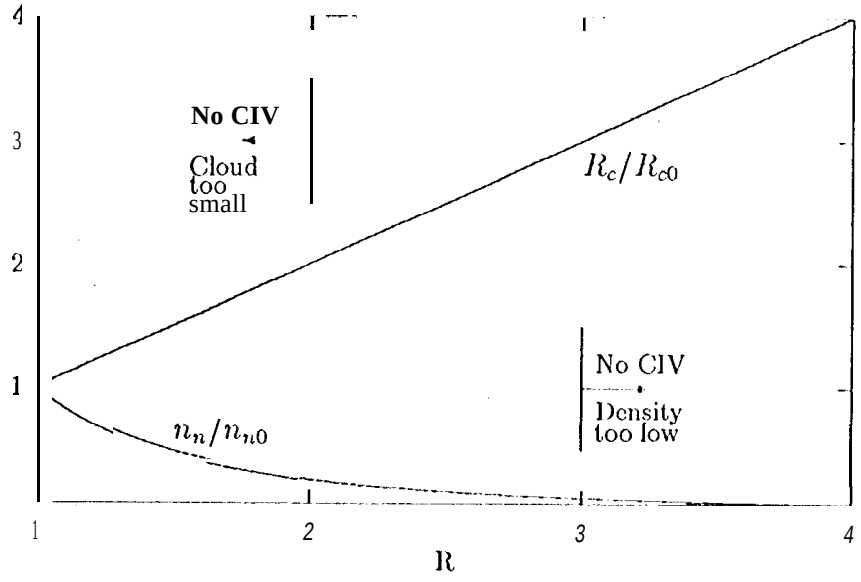
4
3
2
1
No CIV
Cloud
too
small
R_c/R_{c0}
No CIV
Density
too low
n_n/n_{n0}
1
2
3
4
R

Figure 7